Universality of the shear viscosity of alkali metals

N. Meyer, H. Xu, and J.-F. Wax*

Laboratoire de Chimie et de Physique - A2MC, Université de Lorraine - Metz, 1, boulevard Arago 57078 Metz Cedex 3, France

(Received 8 March 2017; revised manuscript received 28 July 2017; published 1 September 2017)

The universality of the shear viscosity of alkali metals is studied up to high pressure. Equilibrium molecular dynamics simulations are used to calculate the stress autocorrelation function, which allows us to obtain the value of shear viscosity using the Green-Kubo formula. Atomic interactions are computed from Fiolhais pseudopotential and are validated by comparison between pair distribution functions and mean-squared displacements obtained from classical and *ab initio* molecular dynamics simulations. The description of the interactions is accurate at least up to 12 GPa, 9.4 GPa, 6.6 GPa, and 3 GPa for Na, K, Rb, and Cs, respectively, and to a lesser extent up to 4.8 GPa for Li. A good agreement between simulation and experimental viscosity results along the liquid-gas coexistence curve is found. The viscosity appears to be a universal property over a wide range of the liquid phase of the phase diagram, between 0.85 and 1.5 times the ambient melting density and up to seven times the ambient melting temperature. Scaling laws are proposed following relations formulated in [Meyer, Xu, and Wax, Phys. Rev. B **93**, 214203 (2016)] so that it is possible to predict the viscosity value of any alkali metal with an accuracy better than 10% over the corresponding density and temperature range.

DOI: 10.1103/PhysRevB.96.094201

I. INTRODUCTION

Over the last decade, the high pressure topic has become considerably attractive, especially in the case of alkali metals because they undergo several structural transformations [1,2] under very high pressure. Strikingly, it even happens that Na becomes transparent at about 200 GPa [3]. At ambient conditions, alkali metals are considered as simple ones whereas application of high pressures induces changes in the electronic distribution which turns to nonspherical. Given these changes, numerous studies on structural transformations under pressure were done, but rarely on other physical properties.

Among the properties that are not investigated under high pressure is the shear viscosity. Indeed, the viscosity of alkali metals has never been studied experimentally beyond normal pressure conditions. However, for some technological issues such as the use of alkali metals as heat transfer fluid in nuclear power plants [4] or for geophysical purposes where liquid alkali are models of the earth's core [5], it is necessary to know the behavior of the viscosity of alkali elements with respect to the different state variables such as temperature, pressure, or density. Measuring viscosity at such pressures or temperatures still remains impossible for the moment, except a few noticeable feats like Ref. [6] (see also references therein) on Fe and Fe-S up to 6.4 GPa. Moreover, alkali metals react chemically and their viscosity is very low (lower than water); this induces additional difficulties.

An interesting feature of the group of alkali metals is the universality of some properties such as static [7] and dynamic structure [8,9] or the self-diffusion coefficient [10,11] along the liquid-gas coexistence curve. Beyond a qualitative analogy of their behavior, these studies have demonstrated the existence of real quantitative scaling properties between the alkali metals. In the present study, the universality of the shear viscosity of Li, Na, K, Rb, and Cs is investigated. If confirmed, such a property would be interesting as it would allow to quantitatively estimate the viscosity of any alkali metal from the knowledge of the data for one of them. This issue was already suggested by Kaptay [12], but for all the metals of the periodic table and at ambient pressure.

Taking into account the thermodynamic conditions considered, numerical simulation appears to be an efficient predictive tool and permits to develop models useful to conveniently determine the viscosity value. In our previous work on Na [13], we explored a wide range of the liquid phase of this system. We also studied K and Cs [14] and revealed a qualitative analogy between the viscosity of these elements. Along isochoric lines, viscosity presents a minimum as temperature increases, except at the lowest densities investigated. On the other hand, it monotonically increases along isotherms.

Furthermore, we proposed relations [13], which qualitatively and quantitatively describe the viscosity of liquid sodium, even up to high densities corresponding to pressures about 12 GPa. The behavior of viscosity η versus temperature T is well reproduced by

$$\eta(T) = (AT^2 + C)e^{B/T}, \tag{1}$$

where A, B, and C are parameters depending on the density. By replacing parameters A, B, and C by their expressions as functions of the density ρ in Eq. (1), we obtained

$$\eta(\rho,T) = \left[\left(\frac{\alpha_A}{\rho^2} + \beta_A\right)T^2 + (\alpha_C + \beta_C\rho)\right]e^{(\frac{\alpha_B}{\rho^2}+\beta_B)/T}, \tag{2}$$

where αs and βs are parameters characteristic of sodium. Finally, when T is kept constant and by rearranging terms in Eq. (2), we obtained the following dependence on density:

$$\eta(\rho) = \left(\frac{a}{\rho^2} + b + c\,\rho\right)e^{d/\rho^2}, \tag{3}$$

where a, b, c, and d are temperature dependent parameters. In this study, the shear viscosity is simulated for the five alkali metals. This collective property is calculated from the stress autocorrelation function (SACF) using the Green-Kubo relation. The correlation functions are computed from microscopic configurations generated by molecular dynamics (MD) simulations.

*Corresponding author: jean-francois.wax@univ-lorraine.fr

Classical simulations imply getting accurate atomic interactions in order to realistically describe the properties of the material. It is *a fortiori* true in the case of metallic materials where the density strongly influences the interactions. Usually, alkali metals are studied at ambient conditions with an effective pair potential because the electronic structure is simple. Each atom has only one valence electron which is only loosely bound, that induces a monatomic structure with a homogeneous cloud of nearly-free electrons. However, above the normal pressure, it is commonly accepted that *ab initio* methods are more reliable because alkali metals have very nonuniform and nonspherical distribution of electron density around ions that does not allow the application of spherical effective pair potentials at high pressures anymore. However, in fact, the use of an effective pair potential derived from Fiolhais pseudopotential [15] still remains possible up to a certain density, as shown in Ref. [13]. *Ab initio* simulations are more accurate, but much more demanding from the computation time point of view. This prohibits the extensive study of some properties such as the shear viscosity which requires a rather long simulated time in order to improve statistical accuracy.

Consequently, in this study, our simulations are performed using Fiolhais potential. Nevertheless, we will first confirm the reliability of the description of the interactions for the five alkali metals up to a certain density/pressure by comparing the pair distribution functions and mean-squared displacements (MSD) obtained from our MD simulations with those from *ab initio*. The only available experimental data for viscosity are obtained at ambient conditions and we will check the agreement with our simulations. Then, in order to investigate the universality of the viscosity, we will extend the study to reduced thermodynamics states for Li, Na, K, Rb, and Cs, namely, along three isochoric lines (0.75 ρ_m, ρ_m, 1.5 ρ_m) and along an isotherm (4.3 T_m) where ρ_m and T_m denote the density and temperature at the melting point under ambient pressure. In order to demonstrate the universal behavior of the viscosity, we will then define reduced quantities to reveal scaling laws. The possibility to determine the viscosity of any alkali metal from the known viscosity of only one will be discussed.

This paper is laid out as follows. Section II is devoted to the description of phase diagrams of each alkali metal from the literature data. We will point out the analogies and differences that exist. In Sec. III, the formalism is developed. We will give relevant computational details in order to obtain the shear viscosity from the SACF and check the validity of Fiolhais potential, essential ingredient in the use of MD simulation. In Sec. IV, we will analyze the results of shear viscosity for Li, Na, K, Rb, and Cs. A comparison with experimental data available in the literature will be done. Then, the temperature and density dependence of the viscosity will be qualitatively discussed. Lastly, we will examine the issue of its quantitative universality. Finally, in Sec. V, we will give the conclusions and the perspectives of this work.

II. UNIVERSALITY OF PHASE DIAGRAM

Observing a universal behavior among several systems presupposes that some thermodynamic states of these different

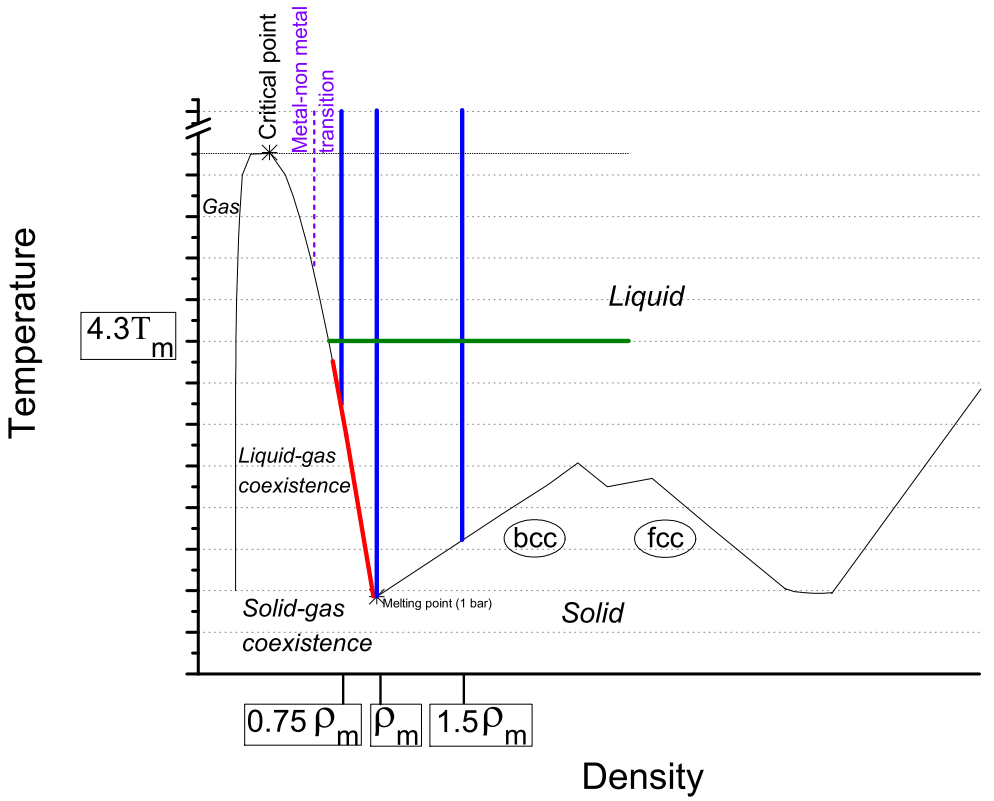

FIG. 1. Schematic universal phase diagram of alkali metals. Thick solid lines correspond to the investigated state points. The red one is along the liquid-gas coexistence curve, while the green and blue ones correspond to an isotherm at 4.3 T_m and 3 isochoric lines (0.75 ρ_m, ρ_m, 1.5 ρ_m), respectively. Thin solid black lines separate transitions between two different phases.

TABLE I. Experimental melting [16] and critical [17] points values of alkali elements.

	T_m (K)	T_c (K)	ρ_m (kg m^{-3})	ρ_c (kg m^{-3})	T_c/T_m	ρ_c/ρ_m
Li	453	3500	519	118	7.73	0.227
Na	371	2508	925	230	6.76	0.249
K	337	2239	829	192	6.64	0.231
Rb	312	2017	1459	290	6.46	0.198
Cs	301	1924	1835	380	6.39	0.207

systems can be considered as equivalent. Therefore we first compare the phase diagrams of the five alkali metals in order to point out the similarities and differences as well.

Degtyareva [1] summarized the sequences of structural transformations on pressure increase for all the alkali elements. From these observations, we can find similarities that we schematize in a universal (T, ρ) phase diagram in Fig. 1. The solid, liquid, and gas phases are separated by thin solid lines. At low densities, the liquid-gas coexistence is recovered with a critical point corresponding to temperatures higher than 1900 K. The critical and melting points of the five alkali elements are summarized in Table I. For all alkali metals, a metal-nonmetal (M-NM) transition is observed at about 2 ρ_c [18]. In order to remain in the metallic region, densities lower than $2.5\rho_c$ will not be investigated in our study.

At ambient conditions, alkali metals are considered as simple because they only have one valence electron and crystallize in the body-centered cubic (bcc) structure type. Under pressure, they transform first into face-centered cubic (fcc) structure. On further compression, a wide variety of more or less complex phases has been observed and reviewed in recent years.

Considering the melting curve of each element, starting from the melting point, a positive gradient is first observed that indicates that the solid phase is denser than the corresponding liquid. Then, two maxima are found (except perhaps for Na where the second one is under debate), which separate the structural transition from a bcc to a fcc crystal. These maxima correspond to temperatures lower than T_c. Then, the curve has a negative gradient meaning that the liquid phase is denser than the solid fcc one. At higher pressure, the fcc structure transforms into more exotic structures. The presence of a minimum corresponds to this transition.

We now can look in more details at each element. Lithium is the lightest and simplest of all the alkali elements (only three electrons and no p electron in the core). At high pressure, a possible analogy with metallic hydrogen [19] could be done which explains part of the broad interest for this element. Recently, the melting curve of Li under pressure was determined by x-ray diffraction [20] and electrical resistivity measurements [21]. From the melting point, a positive slope of the melting temperature is observed up to (10 GPa; 535 K). At this pressure, a jump in the melting temperature is noted [21] and could indicate the structural phase transition bcc-fcc. From 11 GPa, the melting temperature declines sharply when the underlying solid is in the fcc phase, down to a minimum located at (190 K; 40 GPa) or at 310 K according to Refs. [20] or [21], respectively. Then, these two studies showed that this minimum extents over a broad pressure range between 40–64 GPa. Consequently, the general trend of the melting temperature is the same and the difference in the minimum temperature could come from the cooling speeds of samples, which could be different and might form glassy states [22].

Concerning sodium, its melting curve is drawn in the thesis of Mc Bride [2] from the studies of Gregoryanz *et al.* [23] and Marques *et al.* [24]. As the pressure increases, solid sodium undergoes a structural transition from a bcc to a fcc crystal. A pressure-induced drop of the melting temperature from 1000 K at approximately 30 GPa down to room temperature at more than 100 GPa was predicted by simulation [25] and confirmed experimentally [26]. At higher pressures, the temperature of the liquid-solid transition is thought to increase again and solid sodium is thought to undergo further transitions to more exotic structures.

The phase diagram of potassium is drawn up to 22 GPa by Narygina *et al.* [27]. From the melting point, the positive gradient of the melting temperature plateaus at (5.8 GPa; 550 K). The melting curve decreases up to the bcc-fcc-liquid triple point found at (13.6 GPa; 466 K). For pressures higher than this point, the melting temperature remains constant up to 15.6 GPa. Further pressure increase induces a negative slope up to a clear minimum (19 GPa; 390 K).

Among the alkali group, the phase diagram of rubidium is the least well known and the last melting study dates back to 1986 [28]. Two melting maxima in the bcc phase were found at (7 GPa; 550 K) and (11 GPa; 520 K). Between those, the bcc-fcc-liquid triple point was located at (9.5 GPa; 500 K). After the second maximum, a decrease of the melting temperature was observed down to a minimum which could be at about (13 GPa; 500 K). After that, the melting temperature may continue to rise.

In the work of Falconi *et al.* [29], the phase diagram of cesium is presented in the (T, P) plane. The Cs melting curve shows drastic changes in slope with pressure. A positive slope followed by two maxima at (2.25 GPa; 470 K) and (3.05 GPa; 471 K) was found. Further increase of the pressure induces a strongly negative slope of the melting curve until (4.2 GPa; 361 K) it becomes strongly positive again. This study reached the highest pressure investigated by experimental measurements, equivalent to 9.8 GPa.

So, a common shape of the phase diagrams emerges from this description even if differences can be observed on a quantitative point of view (see T_c/T_m or ρ_c/ρ_m values, for instance).

III. FORMALISM

A. Simulation method

From MD simulations, we obtain atomic trajectories and velocities of each particle. This allows to calculate the instantaneous stress-tensor elements $\sigma_{\alpha\beta}(t) = \overline{\sigma_{\alpha\beta}} + \delta\sigma_{\alpha\beta}(t)$. Using the Green-Kubo relation, by integration of the time-autocorrelation function of the off-diagonal elements of the stress tensor, the value of the shear viscosity is obtained as

$$\eta_{\alpha\beta} = \frac{V}{k_B T} \int_0^\infty \langle \delta\sigma_{\alpha\beta}(0)\delta\sigma_{\alpha\beta}(t)\rangle dt, \qquad (4)$$

where V is the volume of the system, T, its temperature, k_B, Boltzmann's constant. Notation $\langle \dots \rangle$ refers to an average

over a sufficiently large number of phase-space trajectories in order to reach the thermodynamic mean and $\langle \delta\sigma_{\alpha\beta}(0).\delta\sigma_{\alpha\beta}(t)\rangle$ is called the stress autocorrelation function (SACF). $\delta\sigma_{\alpha\beta}(t)$ denotes the fluctuating part of the instantaneous $\alpha\beta$ component of the stress tensor (with $\alpha,\beta = x,y,z$) [30]

$$\sigma_{\alpha\beta}(t) = -\frac{1}{V}\left(\sum_{i=1}^{N} m_i(\mathbf{v}_i)_\alpha(\mathbf{v}_i)_\beta + \sum_{i=1}^{N-1}\sum_{j>1}^{N}(\mathbf{r}_{ij})_\alpha(\mathbf{f}_{ij})_\beta\right) + \sigma^{(0)}_{\alpha\beta}(\rho,T). \quad (5)$$

In this expression, $\sigma^{(0)}_{\alpha\beta}(\rho,T)$ is a density dependent term that is specific to metals as it stems from the electron gas and is nonzero only for diagonal terms (see Appendix). The two other contributions have kinetic and interatomic origins. Note that in the thermodynamic limit, the diagonal terms, $-\overline{\sigma_{\alpha\alpha}}$, identify with the pressure, while the off-diagonal terms, $-\overline{\sigma_{\alpha\beta}}$, are zero.

Equilibrium simulations were carried out in the microcanonical NVE ensemble, in which the number of particles, N, the volume and the total energy E of the system are keep constant. Cubic simulation boxes of side L contained 2048 atoms and their walls were replaced by periodic boundary conditions. The interaction cutoff radius was chosen at the position of the node of the force directly smaller than $L/2$, in order to limit truncation errors. To calculate the trajectories and velocities of the particles, Verlet's algorithm in its velocity form was used to solve Newton's equations of motion.

To reach the required accuracy when computing the viscosity, an important computational effort is required. 6 000 000 production steps corresponding to at least 1 ns depending on the metals appeared to be large enough a number to sample the whole phase-space. In order to reduce the strong fluctuations of the SACF and improve its convergence, three techniques were used. (1) We considered a large number of time origins [at least 590 000 in Eq. (4)]. (2) An average was done over three off-diagonal elements of the stress tensor σ_{xy}, σ_{yz}, σ_{xz}, and three directions obtained by 45° rotations of the axes, namely $\frac{1}{2}(\sigma_{xx} - \sigma_{yy})$, $\frac{1}{2}(\sigma_{yy} - \sigma_{zz})$, and $\frac{1}{2}(\sigma_{xx} - \sigma_{zz})$. (3) Eight independent microscopic states corresponding to the same macroscopic state point were considered. Thus we reach an uncertainty of less than 5%. For further details about this point, please refer to our previous work [13] where the method for viscosity calculation is exactly the same and developed in more details.

For calculations on alkali metals, Fiolhais potential [15] has been chosen. From a perturbation development of the energy and using self-consistent screening, the effective pair potential can be written as

$$u(r) = \frac{Z^2}{r}\left[1 - \frac{2}{\pi}\int_0^\infty F_N(q)\frac{\sin qr}{q}dq\right], \quad (6)$$

which comprises a direct Coulombic repulsion between ions of valency Z plus an indirect attraction involving the electron gas. This last term is expressed using the energy-wave number characteristic

$$F_N(q) = \left(\frac{q^2}{4\pi}\right)^2 \frac{1}{Z^2}w^2(q)\left[1 - \frac{1}{\varepsilon(q)}\right][1 - G(q)], \quad (7)$$

accounting for the electron-ion interactions [$w(q)$, Fiolhais pseudopotential] and the electron-electron contribution [$\varepsilon(q)$ and $G(q)$, screening functions]. It is responsible for the density dependence of the effective pair potential $u(r)$. This explains why MD simulations at constant pressure can not easily be undertaken. Complete analytical expressions, as well as references to earlier studies, can be found in Ref. [31].

B. Validity of Fiolhais potential

The use of a realistic potential is one of the main conditions to run accurate MD simulations and allows the analysis of properties of real materials such as the shear viscosity. The potential used to describe the atomic interactions in this study was initially developed for the solid state at ambient pressure and has proven its capability to describe the liquid state near the liquid-vapor coexistence [10,31–33]. The lower limit of our interaction model corresponds to the M-NM transition in the low-density direction. Indeed, at about twice the critical density, there is a continuous increase in the electron localization leading to ion clustering [34]. Near or below the critical density, all the conduction electrons are localized and it has been observed the presence of dimers, feature of a dilute gas. Consequently, near the M-NM transition, electronic distribution can not be considered as nearly free anymore and this implies that the self-consistent screening formalism (and consequently Fiolhais potential) can not be used below $2\rho_c$.

On the other hand, for the high densities or pressures, it cannot be stated a priori with certainty that this potential is able to account for these changes. Usually, the liquid metals under very high pressure have nonuniform and especially nonspherical distribution of electron density around ions. The overlapping atoms force their outer electrons into the interstices [3,35], that does not allow the application of self-consistent screening at high pressures.

In order to test the reliability of the interaction description in the high-density range, we considered the following. For each alkali metal, at a density close to the estimated value of the maximum of its melting curve, we performed several classical simulations by increasing gradually the temperature. The MD simulations were initialized with a perfect body-center cubic (bcc) lattice structure at a temperature slightly below the melting temperature. The temperature was increased gradually until melting in order to determine the transition temperature by considering the MSD. At each temperature, the thermalization stage lasted 60 000 time steps and the production stage 90 000. Even if superheating is expected to occur, the renormalization of the velocities during the thermalization stage strongly reduces the extent of the phenomenon [36].

Then, in the liquid state, we compared the pair distribution function, $g(r)$, obtained with our model to *ab initio* molecular dynamics (AIMD) simulations. For Li, Na, and Rb, $g(r)$ from AIMD results at high pressure were found in the literature [37–39] where the atomic volume or density is indicated, allowing us to perform classical MD simulations at the same density. Concerning K and Cs, there are neither experimental nor *ab initio* studies done at high pressure, which give $g(r)$ or, if they exist, the corresponding densities are not specified. In this context, we performed AIMD simulations

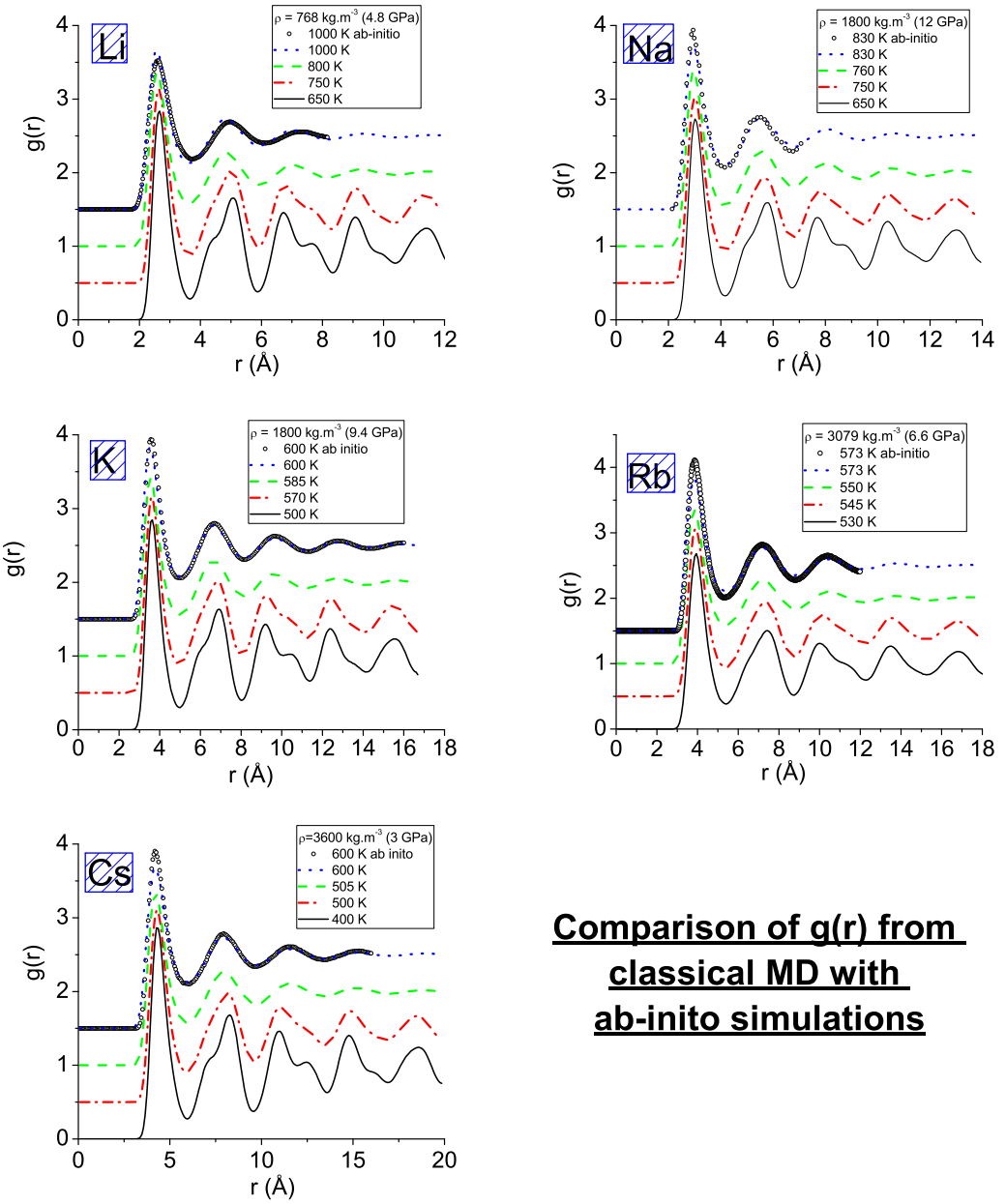

FIG. 2. Validity of Fiolhais potential at high densities. Pair distribution function, $g(r)$, at several temperatures. Classical MD results of $g(r)$ are also compared with AIMD in order to check the reliability of the description of the interactions. Lines correspond to data obtained from classical MD simulations while circles are AIMD results. *Ab initio* simulations are performed in this study for K and Cs, whereas data of Li, Na, and Rb are those of Refs. [37–39]. Red, green, and blue curves of $g(r)$ are shifted 0.5, 1, and 1.5 up compared to the black one, respectively. Pressure values correspond to AIMD simulations.

using VASP code [40] with 300 atoms at a temperature of 600 K for K and Cs in canonical NVT ensemble. After thermalization stage, the production lasted 10 000 time steps 3-fs long in order to compute $g(r)$ and check that the system is liquid. We used projector-augmented-wave (PAW) pseudopotentials [41] treating p and s semi-core states as valence states. Exchange and correlation were described within the generalized gradient approximation (GGA) using the PBE functional [42].

The pair distribution functions, $g(r)$, are plotted in Fig. 2 and the MSD in Fig. 3 along the isochoric line corresponding to density 768, 1800, 1800, 3079, and 3600 kg m^{-3} for Li, Na, K, Rb, and Cs, respectively. We observe that the effective pair potentials recover the AIMD results of $g(r)$ at temperatures where the metal is liquid. Except a small phase shift in the case of Li, the agreement is excellent between the predictions of both kinds of simulations. We also plot the MSD obtained from our *ab initio* simulations of K and Cs (Fig. 3). The agreement is only qualitative. We recall that self-diffusion coefficient related to the MSD slope is very sensitive to the temperature. Surely, most of the difference can be attributed to the interactions even if differences between the way simulations are performed (statistical ensemble, size, time step, ...) should also be considered.

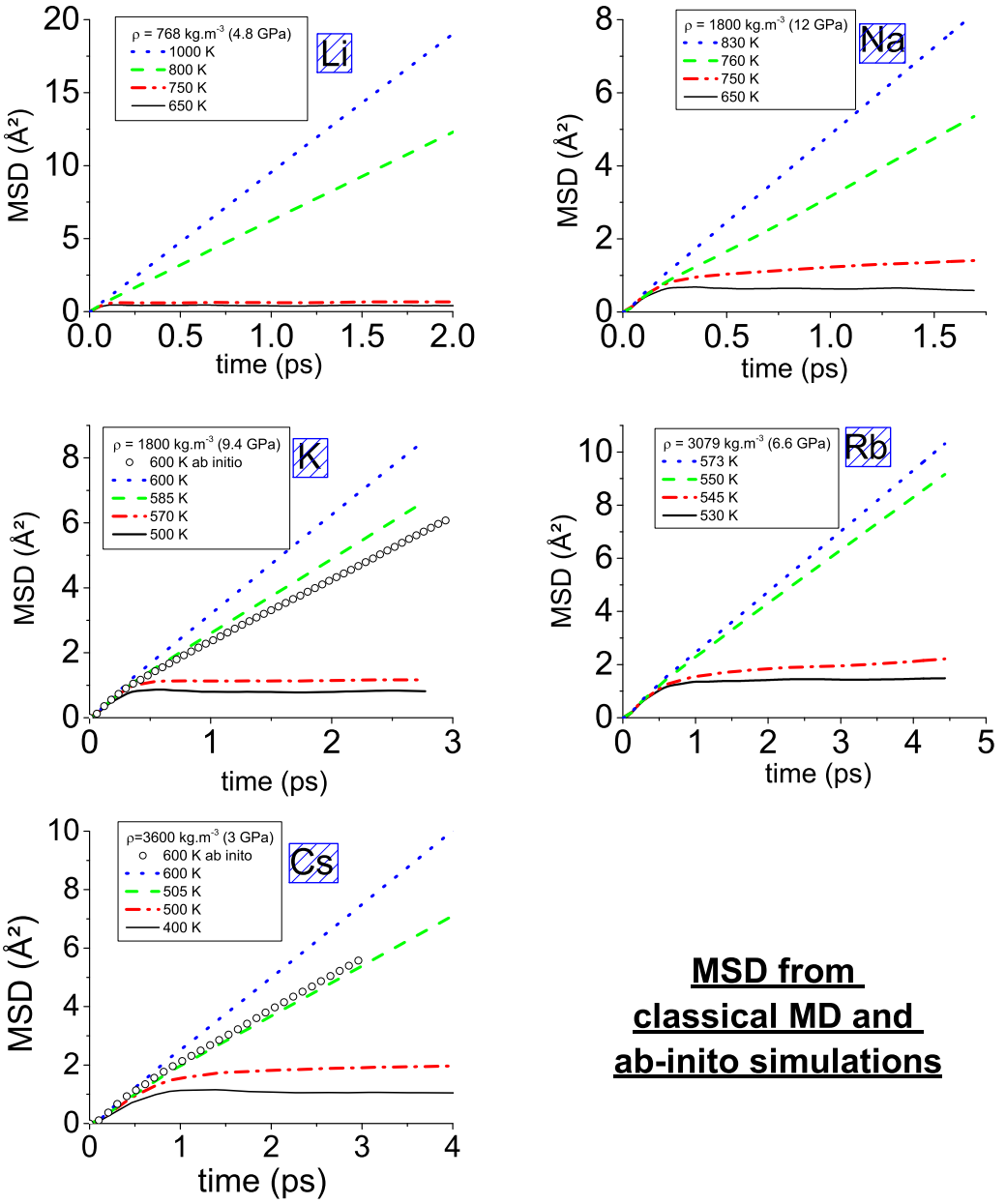

FIG. 3. Validity of Fiolhais potential at high densities. For each element, mean-squared displacement are displayed at several temperatures in order to evaluate the melting temperature. Same legend as in Fig. 2 for $g(r)$.

At these densities, we observe melting between [750–800 K], [750–760 K], [570–585 K], [545–550 K], [500–505 K] for Li, Na, K, Rb, and Cs, respectively. To our knowledge, the only available data of density at the melting temperature as a function of pressure are those provided by *ab initio* simulations. Na is well documented (see Ref. [13]), but not the other alkali metals so that performance of our potentials in determining the melting temperature can only be evaluated indirectly. Looking for instance at Cs, the experimental melting curve plateaus at 470 K between 2.25 and 3.05 GPa. At 3600 kg m^{-3} and 600 K, *ab initio* simulations predict that it is liquid at a pressure of 3 GPa. Thus it is reasonable to believe that this density is part of the plateau. At this density, Fiolhais potential estimates the melting temperature between 500 and 505 K. Considering the existence of overheating, we can assert that the agreement with experimental data is probably good. Such an argument is effective for K, Rb, and Cs, but not for Li. As for Na, it has already been discussed favorably in Ref. [13].

The pressures estimated from AIMD simulations (see Table II) are consistent with the experimental phase diagram data reported above. With density-dependent potentials, the evaluation of pressure has to be performed carefully. Indeed, additional terms appear in its expression due to the existence of the electron gas. To cut the long story short (see Appendix for more details), the energy reads

$$E = E_k + U(V) + U(R,V)$$
$$= \frac{3}{2}Nk_BT + Nu_0(n) + 2\pi N\rho_N \int_0^\infty r^2 u(r,n)g(r)dr, \quad (8)$$

TABLE II. Pressure corresponding to the thermodynamic states at which AIMD simulations are performed. Top part corresponds to classical MD simulations with Fiolhais pseudopotential: P_{id}, P_0, and P_{i-i} are contributions to the total pressure, P_{Fiol}. Bottom part compares AIMD (P_{AIMD}) and classical MD values obtained from Eq. 9 (P_{Fiol}) and from the stress-tensor (P_{xyz}).

	T (K)	ρ (kg m^{-3})	P_{id} (GPa)	P_0 (GPa)	P_{i-i} (GPa)	P_{Fiol} (GPa)
Li	1000	768	0.92	−7.60	19.88	13.20
Na	830	1800	0.54	−4.17	16.49	12.86
K	600	1800	0.23	−2.72	10.85	8.36
Rb	573	3079	0.17	−1.93	7.58	5.82
Cs	600	3600	0.13	−1.39	4.91	3.63
	T (K)	ρ (kg m^{-3})	P_{AIMD} (GPa)	P_{Fiol} (GPa)	P_{xyz} (GPa)	$P_{xyz} + P_0$ (GPa)
Li	1000	768	4.8	13.20	19.98	12.38
Na	830	1800	12	12.86	17.08	12.91
K	600	1800	9.4	8.36	10.86	8.13
Rb	573	3079	6.6	5.82	7.30	5.37
Cs	600	3600	3	3.63	4.87	3.48

where ρ_N and n are the atomic and electronic densities, respectively. In this expression, the term $U(V)$ is due to the electronic gas, as well as the explicit density dependence of the effective pair potential (which is usually omitted). Consequently, the pressure has the following expression:

$$P = \rho_N k_B T + \rho_N n \frac{du_0}{dn} - \frac{2\pi\rho_N^2}{3} \int_0^\infty r^3 \frac{\partial u(r,n)}{\partial r} g(r) dr + 2\pi\rho_N^2 \int_0^\infty n r^2 \frac{\partial u(r,n)}{\partial n} g(r) dr. \quad (9)$$

In the right-hand side of this equation, the first term is the ideal pressure P_{id}, the second one is volume-dependent and noted P_0, while the last two terms correspond to the structure-dependent part which sum is noted P_{i-i}. For consistency, these last terms are evaluated by taking the cutoff radius of the interactions used in MD simulations into account. As can be seen in Table II, except for lithium, the pressure obtained from our description of the interactions is close to the AIMD value. So, we believe that, except for Li, the melting temperature is well predicted by our description of the interactions.

The pressure may also be obtained from the diagonal elements of the stress-tensor. However, as can be seen in Table II, care must be taken as the volume-dependent contribution P_0 must be accounted for. Anyway, this does not prevent us to compute the viscosity from the diagonal terms as the this contribution vanishes when computing difference such as $P_{xx} - P_{yy}$.

Our previous study of sodium had already shown the validity of Fiolhais potential even in the high-density region for this element and we can draw the same conclusion for the other alkali metals. We consider that our interaction description is reliable up to the highest density investigated. At higher densities and pressures, electron localization appears which is not compatible with self-consistent screening. This corresponds to the upper limit of our interaction model. Consequently, the investigated thermodynamic states are all located below the pressure where the structure and physical properties of liquid alkali metals are expected to change, namely, 60 GPa [43] for Na, 19 GPa [27] for K, 12.5 GPa [37] for Rb, and 3.9 GPa [29,44] for Cs. They are represented schematically in Fig. 1. The red line corresponds to the liquid-gas coexistence. Three isochors were studied (blue lines): at the density of the melting point ρ_m, at a lower density corresponding to 0.75 ρ_m, and at a higher one equal to 1.5 ρ_m. The temperature ranges from the liquid-gas coexistence curve at 0.75 ρ_m or in other cases from the melting curve, up to 7000 K. For the density dependence, we investigated state points along an isotherm (green line) with density ranging from the liquid-gas coexistence limit up to 2 ρ_m. To summarize, Fiolhais potential can accurately describe the behavior above the M-NM transition and up to at least 12, 9.4, 6.6, and 3 GPa for Na, K, Rb, and Cs, respectively, and to a lesser extent up to 4.8 GPa for Li.

IV. RESULTS

We turn now to the presentation of our results which we will especially discuss in the scope of the universality issue.

A. Comparison with experimental data

Before discussing the universality of the shear viscosity between alkali metals, we compare our results with experimental data available in the literature in Fig. 4 for each metal. Red circles correspond in each case to the simulations while the color symbols are the measurements. These experimental data were obtained under atmospheric pressure, i.e., close to the liquid-gas coexistence line. Our simulations were performed along this line.

In each case, a shift clearly appears between experimental and simulated data, of the order of 40% for Li (compared to Novikov's data [45]), 18% for Na (Ewing [49]), 25.8% for K (Lemmon [51]), 9% for Rb (Genrikh [54]), and 21.5% for Cs (Tsai [55]). Due to the very low viscosity of alkali metals, these relative differences seem to be rather high, but in fact the difference is only about 4×10^{-5} Pa s for Na, K, Rb, and Cs.

Inaccuracies in the description of the interactions may be one of the reasons for this difference and it could also explain why the melting temperature found for Li is in slightly worse agreement with the experimental one. Nevertheless, it should be recalled that due to chemical reactivity of alkali elements, the viscosity is indirectly measured from the

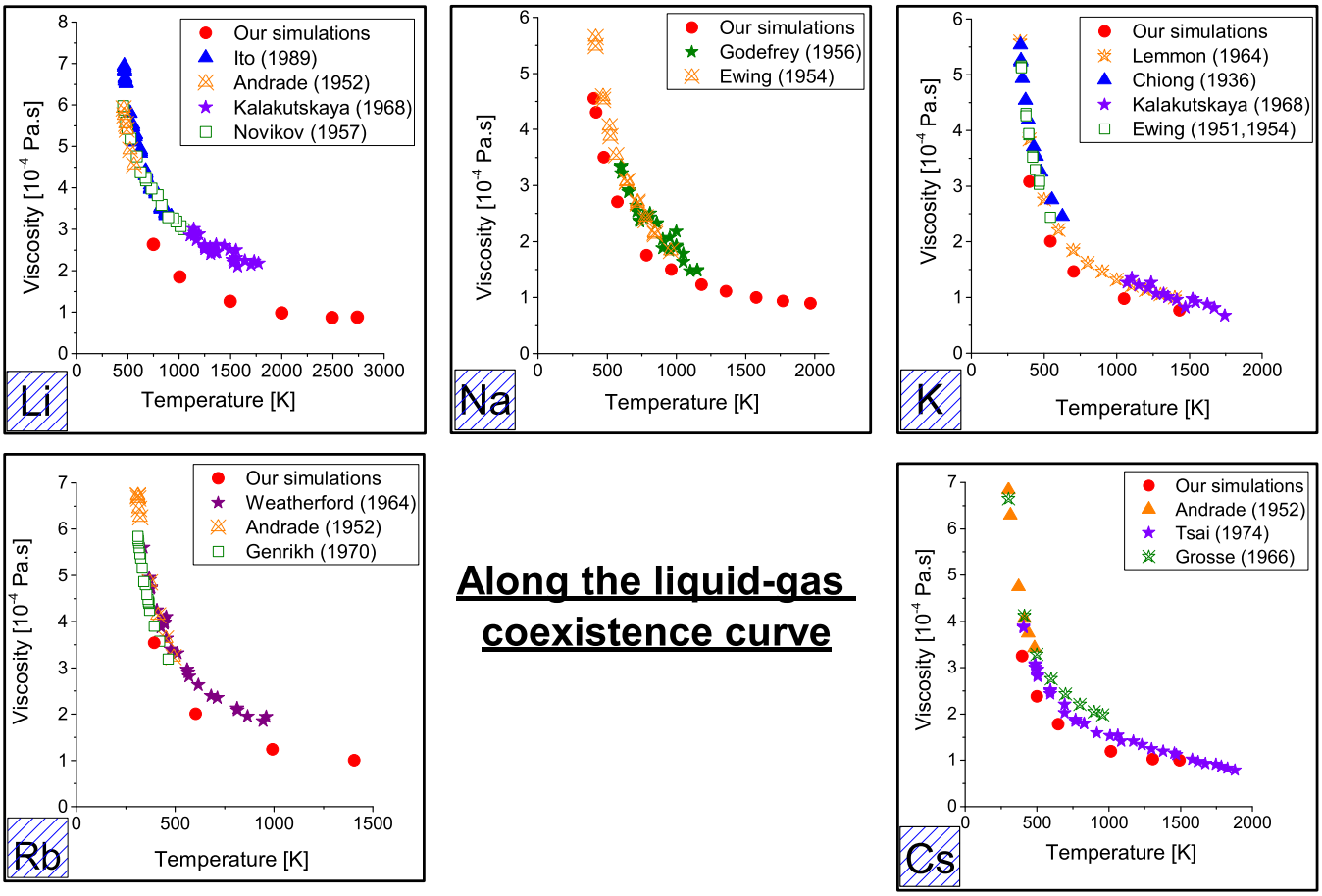

FIG. 4. Viscosity as a function of temperature along the liquid-gas coexistence for Li, Na, K, Rb, and Cs. Comparison between experimental data and our simulation results (red circles). For Li, Novikov [45], Kalakutskaya [46], Andrade [47], and Ito's [48] data are represented by squares, stars, X-triangles, and triangles, respectively. For Na, X-triangles and stars correspond to Ewing [49] and Godfrey's data [50]. For K, Lemmon [51], Chiong [52], Kalakutskaya [46], and Ewing's data [49] are symbolized by X-triangles, triangles, stars, and squares, respectively. For Rb, Weatherford [53], Andrade [47], and Genrikh's [54] data correspond to stars, X-triangles, and squares. Lastly, measurements for Cs were done by Andrade [47] (triangles), Tsai [55] (stars), and Grosse [56] (X-stars).

damping of the oscillations of a container filled with fluid. These measurements are very delicate and, surprisingly, date back to the 1970's for the most recent (apart from Ref. [48], to the best of our knowledge). Moreover, some studies showed that the viscosity of liquid metals is very sensitive to metallic impurities [57] or to the presence of air introduced into the atmosphere over the metal (gaseous impurities) [54]. For instance, an oxygen concentration of 0.15 wt.% in Rb leads to an increase of 20% of the viscosity. Except Genrikh *et al.* [54], authors did not take specific measures to purify the metal of gaseous impurities. The occurrence of these impurities, particularly atmospheric oxygen, might have caused part of the difference between our data and those in the literature. Thus it could explain why taking into account the viscosity values of Genrikh, the relative difference is much smaller for Rb contrary to other metals. Consequently, even if the pair potential is certainly the most important source of discrepancies, an updating of the experimental measurements of the viscosity of these metals is clearly needed. However, lithium differs from others and shows a greater discrepancy. As it has already been mentioned above, this difference could be related to its unique electronic structure (no p electron in the core).

On the other hand, notwithstanding the above-mentioned shift, our data nicely reproduce the variation of the viscosity along this line and we believe that they are appropriate to discuss temperature and density dependence of this physical quantity.

B. Qualitative analysis

Similar qualitative behaviors of the viscosity of the different elements is a necessary condition for universality. In panel (a) of Fig. 5, the temperature dependence of the shear viscosity of all alkali metals is studied along three well specified isochoric lines: 0.75 ρ_m, ρ_m, 1.5 ρ_m. For densities equal or higher than ρ_m, the same qualitative behavior of the viscosity is found for all elements. As temperature increases, viscosity decreases quickly at lower temperatures, reaches a minimum, and increases slowly in the high-temperature region. In the low-temperature region, near freezing, the viscosity is determined mainly by interaction effects. As the temperature increases, these effects go down and η is determined by the kinetics of pair collisions. The minimum is predicted to occur in the intermediate region. This behavior has been discussed in

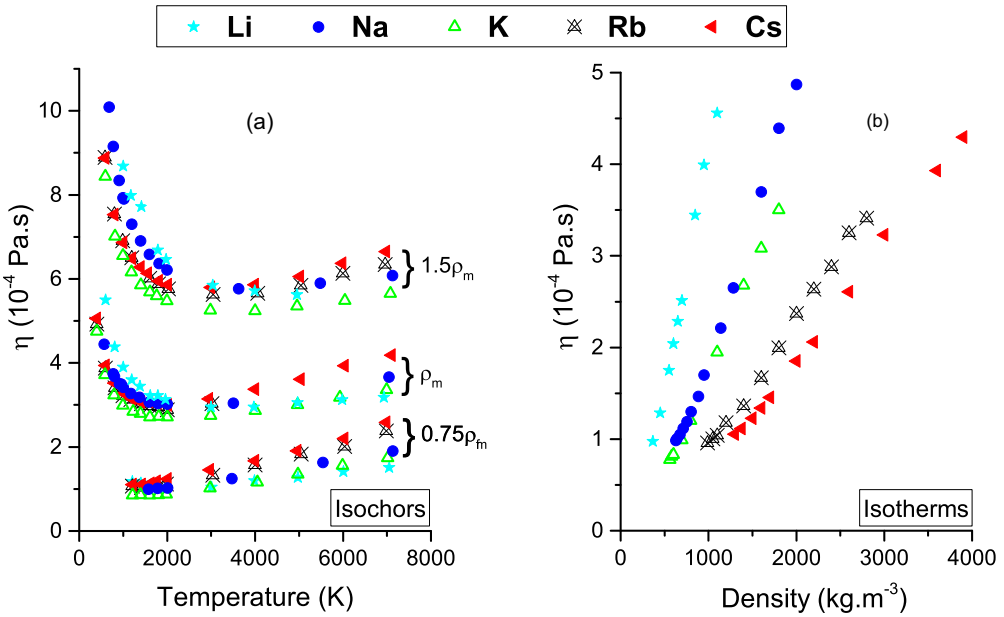

FIG. 5. Viscosity of Li (stars), Na (circles), K (triangles), Rb (X-triangles), and Cs (left-triangles) as a function of temperature along three isochoric lines 0.75 ρ_m, ρ_m, and 1.5 ρ_m (a) and as a function of density along an isotherm 4.3 T_m (b). In (a), curves at ρ_m and 1.5 ρ_m are shifted 1.5×10^{-4} and 3.5×10^{-4} Pa s up, respectively.

details in our study of Na [13] and already confirmed for K and Cs [14]. It has been shown that the occurrence of a minimum which is first counter-intuitive, is not solely typical of alkali metals since the viscosity behaves in the same way in other systems like rare gas at liquid densities [58]. Experimental and simulation studies on argon have shown this feature. Moreover, Rosenfeld [59] predicted a minimum of the viscosity as a function of temperature on the basis of the entropy scaling. At low densities (0.75 ρ_m), we can model this group of isochors by a simple linear low. Indeed, the liquid-gas coexistence line prevents from giving a clear overview of the viscosity behavior at lower temperatures.

In panel (b) of Fig. 5, the density dependence of the shear viscosity of alkali elements is studied along an isotherm corresponding to 4.3 T_m. For all elements, the viscosity increases with the density, due to the increase of atomic interaction effects. In the high-density region, the behavior of the viscosity is linear while viscosity values are not accessible at lower densities due to the liquid-gas coexistence line.

For both kinds of dependence, the same behavior was recovered for each alkali elements. This raises the question of whether a universality exists both for the temperature and for the density dependence on a quantitative level.

C. Universality of the shear viscosity

In order to establish the universality of the viscosity among the alkali metals, we need to define reduced quantities and check if they quantitatively obey the same law. One possible procedure could consist in plotting pair potentials in proper reduced units to state their scalable shapes; then define reduced length and energy units in order to reduce the viscosity. This is what we have done in a former study about self-diffusion coefficient [11]. However, this would only be relevant for people using pair potentials. We prefer to consider more general features that are also meaningful to experimentalists, as well as in the framework of *ab initio* simulations. Thus the proposed relations will be relevant in all these contexts.

Two possible choices can be used to reduce the data: the melting point (T_m, ρ_m) or the critical point (T_c, ρ_c). The viscosity values corresponding to both particular points are summarized for the five alkali metals in Table III.

1. Reduced viscosity

In panel (a) of Fig. 6, the shear viscosity is shown as a function of temperature as obtained in our simulations for Li, Na, K, Rb, and Cs, along the liquid-gas coexistence line. Reduced by the appropriate parameter, i.e., the melting point, we see that there is no doubt about the universality of viscosity of alkali along the coexistence curve. If the viscosity is reduced by the critical point then the curves do not start at the same value of T_m/T_c, given that the ratio is different according to the metals.

In panel (b) of Fig. 6, isotherms are drawn corresponding to 4.3 T_m and reduced by the melting point for Li, Na, K, Rb, and Cs. Once again, an obvious universal behavior of viscosity arises along reduced isotherms up to 1.6 ρ_m. From this density,

TABLE III. Experimental values of the shear viscosity at the melting point for Li [48], Na [52], K [51], Rb (as cited in Ref. [60]), and Cs [47]; estimated values at the critical point from Ref. [17].

	η_m (10^{-4} Pa s)	η_c (10^{-4} Pa s)
Li	6.96	0.62
Na	7.20	0.58
K	5.60	0.49
Rb	6.44	0.62
Cs	6.80	0.64

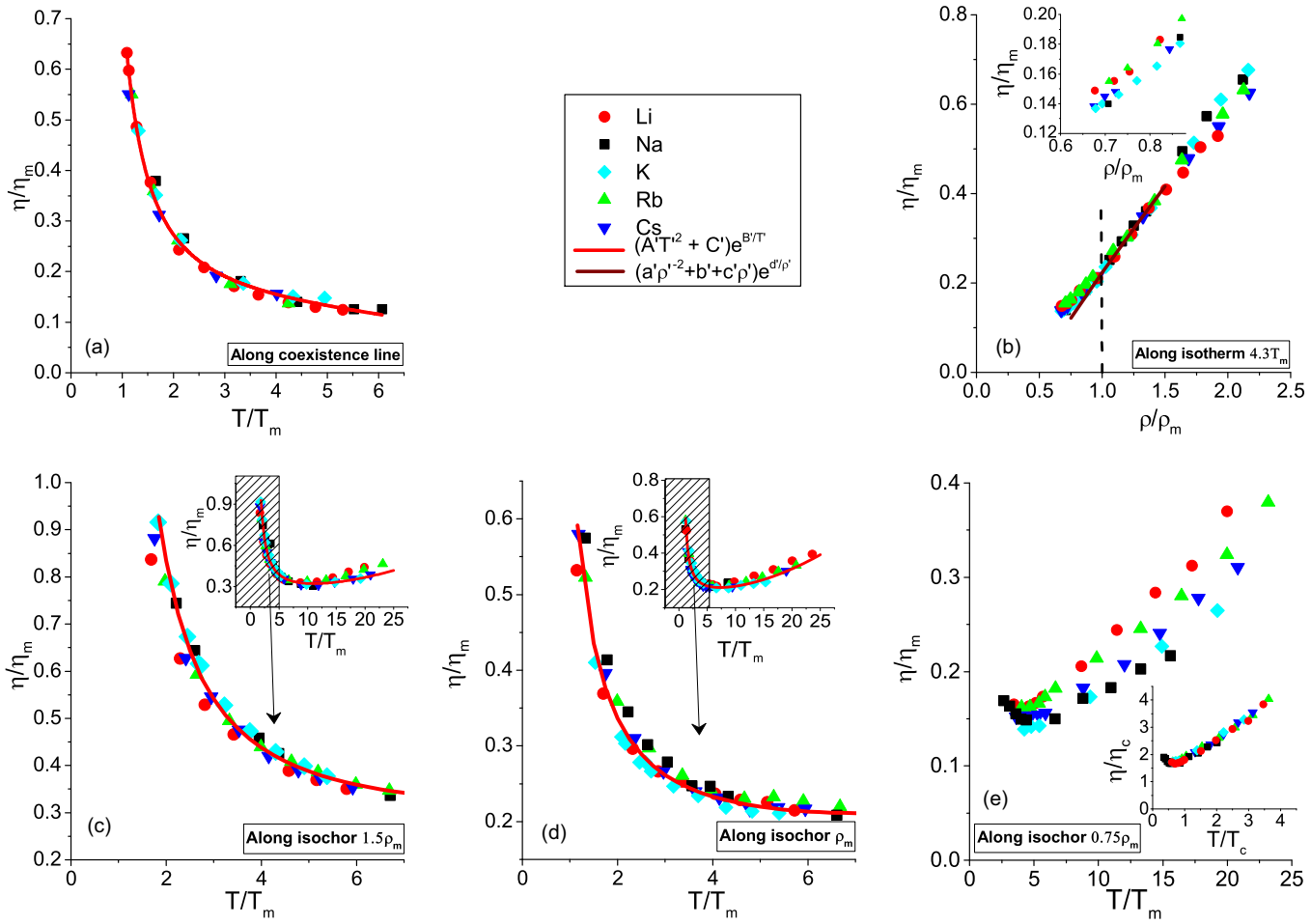

FIG. 6. Reduced viscosity of Li, Na, K, Rb, and Cs. (a), (b), (c), (d), and (e) represent the viscosity values reduced by the melting point along the coexistence line, isotherm 4.3 T_m, and isochors 1.5 ρ_m, ρ_m, and 0.75 ρ_m, respectively. The viscosity values of Li, Na, K, Rb, and Cs, are represented by black squares, sky blue diamonds, blue down-triangles, red circles, and green triangles, respectively. Inset in (b) corresponds to an enlargement of the low-density range, while in (c) and (d), they show the curves over the full temperature range; in (e), it displays the data reduced by the critical point. Solid lines are fit as explained in the text.

the isotherms seem to split into two groups. The lightest metals, lithium, and sodium, tend to separate from the heaviest ones. Even if the phase diagrams of elements are qualitatively the same, they are quantitatively very different at high density. Thus it is not surprising that the splitting occurs in this density range. At ordinary densities, the band structure of alkali metals is free-electron like, but at higher densities their electronic structures depart from this behavior due to the core electrons which start to overlap [61]; this implies changes in the valence electron configuration that may not occur at the same relative pressure/density. The highest densities at which we work are lower than the densities where these electronic transitions occur. Nevertheless, viscosity behavior under pressure could be sensitive to germs of these modifications. Moreover, an *s-d* transition occurs for heavy metals while it is a *s-p* transition for Li and Na [1]. The two kinds of transitions could also be the origin of the separation between light and heavy metals.

Below ρ_m, a splitting is also recovered [see inset of panel (b)]. Its origin could be explained by the fact that, near to the M-NM transition, there are changes in the electronic distribution and the viscosity reflects it. However, the splitting into two groups in this density region is only about 7%. So, the discussion about the universal feature of the viscosity remains relevant.

In panels (c) and (d) of Fig. 6, the simulated viscosity is represented along two well-defined isochors: at the melting density, ρ_m, and at a higher density, 1.5 ρ_m. For both, the viscosity was calculated for Li, Na, K, Rb and Cs, up to 7 000 K. First, it appears that the best way to reduce these data is to draw them as a function of the melting point. We observe that all alkali elements exhibit a clear universality along both isochoric lines, but only within a specific temperature range. Indeed, up to 7 T_m, the behavior of the viscosity is quantitatively the same whatever the metal considered. As cited above, it is mainly the interaction effects which dominate in this range. In the study of Wax *et al.* [10], atomic interactions of alkali metals were calculated using Fiolhais potential and a universal behavior of the diffusion properties was also found near the melting point. Here, the same is observed for viscosity at ρ_m, but also at 1.5 ρ_m.

In the low-temperature range, the potential part prevails over the kinetic one. Looking at the shape of the potential $u(r)$ for the alkali metals (Fig. 7), it could be objected that this is a consequence of the use of the same expression for the

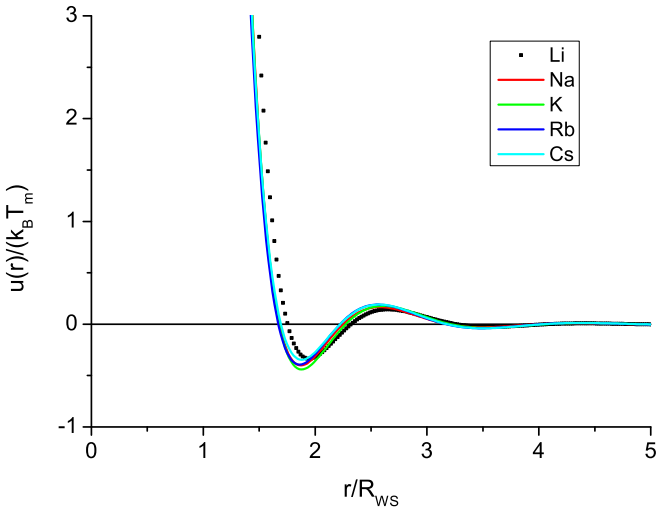

FIG. 7. Effective pair potentials in reduced units at the melting point under ambient pressure; T_m and R_{WS} are the corresponding melting temperature and Wigner-Seitz radius.

pseudopotential, namely that proposed by Fiolhais. Knowing this universal behavior of the interactions of alkali metals, it would not be surprising to recover a universal behavior of the viscosity in this density range. In other words, one may think that the viscosity is universal because the shape of the potential is universal due to the use of the same pseudopotential for all alkali metals. However, in the work of Wax *et al.* [62], Fiolhais pseudopotential has been used to calculate the effective interactions, $u(r)$, of alkaline-earth metals. It has been shown that this potential describes accurately the interactions in these metals, but it appears that there does not exist a universal behavior of $u(r)$. So, Fiolhais potential is not the cause of the scalability of the effective pair interactions (and of the universality of the viscosity) which is a feature of alkali metals. This scalability already mentioned for Fiolhais potential in Ref. [11] was also observed by Balucani *et al.* [8] with Price's pseudopotential.

In contrast, at higher temperatures, the ratio is reversed and the interactions effect becomes negligible compared to the thermal excitation. Given that the kinetic part depends of the particle mass, it explains the small difference of viscosity behaviors at high temperatures between the metals.

Along isochor 0.75 ρ_m [panel (e)], the universal behavior is not quantitatively recovered. This can be attributed to differences in the density and temperature ratios between melting and critical points among the five alkali metals. As a first consequence, in the low-temperature region, the viscosity of the elements seem to follow qualitatively the same behavior but do not coincide. Indeed, as Li has the highest ratio between critical and melting temperatures, this leads to consider lower T/T_m values than for the others. Moreover, the coexistence curves of alkali metals are extremely asymmetric compared to those of rare gases, for instance. This could be due to the "principle of corresponding states" [63], which is not respected in the alkali group since the type of bonding are not similar in the liquid or vapor states. Near the M-NM transition, most of the electrons are attached to their parent atoms, occupying spatially localized atomic orbitals [64].

TABLE IV. Universal parameters of Eq. (10).

	A	B	C
α'	1.814×10^{-4}	-1.900	9.111×10^{-3}
β'	1.633×10^{-4}	3.474	0.143

So, the nature of the electronic interactions between atoms changes with the decrease of the density and the increase of the temperature (along the coexistence curve). Again, the different ratio between critical and melting densities implies that for densities quite low when compared with ρ_m, the M-NM transition may be at a more or less advanced stage, depending on the metal.

Reducing the data with the critical point [inset of panel (e)] leads to a better agreement. However, this may be fortuitous, first because the viscosity at the critical point is only estimated, so that uncertainty about these values is high. Second, the critical points may not be accurately located, specifically for Li where it is the highest among alkali metals. The accuracy of measurements is severely limited by the highly reactive nature at high temperatures, but also by the control and measurement of temperature in any high-temperature experiment. The measure of the temperature becomes particularly difficult close to the critical point due to the presence of spurious effects caused by the temperature gradients [65]. Anyway, in any other situation, reducing data by the critical point leads to results worse than by the melting point.

Consequently, the viscosity has a quantitative universal behavior over a wide range of temperature (up to 7 T_m), of density (up to 1.6 ρ_m). However, it seems not be the case at low densities (lower than $\simeq 0.85\rho_m$), mainly because of the different ratios between critical and melting points which do not permit to accurately define corresponding states between alkali metals.

2. *Universal expression*

As we mentioned before, by universality, we mean that it is possible to define a set of reduced (universal) variables which allow to obtain quantitatively the behavior of the viscosity for any alkali metal in any thermodynamic state. Given the difficulty to measure experimentally the viscosity, this possibility would be helpful as it would allow to evaluate the viscosity of a metal from the data of another one. This should of course also be possible from simulation results.

Considering Eq. (2), which explicitly accounts for temperature and density, and reducing it with respect to the melting point, i.e., introducing the reduced quantities $\eta' = \frac{\eta}{\eta_m}$, $T' = \frac{T}{T_m}$, and $\rho' = \frac{\rho}{\rho_m}$, we obtain

$$\eta'(\rho', T') = \left[\left(\frac{\alpha'_A}{\rho'^2} + \beta'_A\right) T'^2 + (\alpha'_C + \beta'_C \rho')\right] e^{(\frac{\alpha'_B}{\rho'^2} + \beta'_B)/T'}. \tag{10}$$

In this expression, $\alpha'_A = (\alpha_A T_m^2)/(\rho_m^2 \eta_m)$, $\beta'_A = (\beta_A T_m^2)/\eta_m$, $\alpha'_B = \alpha_B/(\rho_m^2 T_m)$, $\beta'_B = \beta_B/T_m$, $\alpha'_C = \alpha_C/\eta_m$, and $\beta'_C = (\beta_C \rho_m)/\eta_m$ are universal parameters valid for any alkali metal, of which values are deduced from our study of sodium [13] and summarized in Table IV.

TABLE V. Values of fit parameters. A', B', and C' are parameters from Eq. (11), while a', b', c', and d' stem from Eq. (12). Except in the case of the coexistence curve where the parameters were obtained by fitting simultaneously the reduced data of the five alkali metals, the values are obtained from α' and β' of Table IV.

	a'	b'	c'	d'
isotherm 4.3 T_m	7.51×10^{-3}	0.0272	0.319	−0.441
	A'	B'	C'	–
coexistence	-5.72×10^{-4}	1.98	0.104	–
isochor ρ_m	3.45×10^{-4}	1.57	0.152	–
isochor 1.5 ρ_m	2.43×10^{-4}	2.63	0.223	–

For states where the viscosity is obtained as a function of temperature, i.e., along isochoric lines, the data set can be fitted by a reduced version of Eq. (1). This equation becomes

$$\eta'(T') = (A'T'^2 + C')\, e^{B'/T'} \tag{11}$$

with $A' = \frac{AT_m^2}{\eta_m}$, $B' = \frac{B}{T_m}$, and $C' = \frac{C}{\eta_m}$, being universal parameters (i.e., independent of the metal) although functions of the reduced density ρ'. Moreover, this expression also works remarkably well along the coexistence line. In this case, A', B', and C' are independent of the density.

For state points along an isotherm, a reduced version of Eq. (3) can be used

$$\eta'(\rho') = (a'\rho'^{-2} + b' + c'\rho')\, e^{d'/\rho'^2}, \tag{12}$$

where $a' = \frac{a}{\rho_m^2\eta_m}$, $b' = \frac{b}{\eta_m}$, $c' = \frac{c\rho_m}{\eta_m}$, and $d' = \frac{d}{\rho_m^2}$, are universal parameters depending only on the temperature.

The values of the parameters for all fitted curves drawn as solid lines in each panel of Fig. 6 are specified in Table V. First, along the liquid-gas coexistence curve, it is possible to find the reduced viscosity value with an uncertainty of 10% for any alkali element. This is very satisfactory given the accuracy with which this property can be measured which is at least of the same order. Second, considering the isochoric lines ρ_m and 1.5 ρ_m in panels (c) and (d), we obtain a reduced viscosity value with an uncertainty less than 10% in both cases for temperatures up to 7 T_m. This corresponds to very high temperatures (higher than 2 500 K), difficult to achieve in the case of viscosity measurements of alkali metals. Anyway, between 7 and 25 T_m, the agreement remains very satisfactory. Lastly, given that the viscosity behavior along the isotherm is universal between ρ_m and 1.6 ρ_m, it is possible to determine the reduced viscosity within this range with 5% uncertainty. Concerning the isochor at 0.75 ρ_m, the great disparity of curves of the five alkali metals does not permit to fit them with a single curve.

So, with the universal parameters obtained from Eqs. (10), (11), or (12), we get a reduced viscosity which permits to recover the viscosity value of any alkali metal along the fitted thermodynamics states. Conversely, if the viscosity of one alkali metal is known in a given thermodynamic state, it is possible to calculate the reduced viscosity, and consequently to estimate the viscosity of any other alkali metal in a corresponding thermodynamic state. In our previous work [14], we studied the viscosity of Na in greater details, investigating many more thermodynamic states than in the present study, and from which we obtained the universal parameters of Table IV. Thus, knowing the respective values of η_m, ρ_m, and T_m of rubidium, for instance, we can calculate that, at $(1.3\rho_m; 5T_m) = (1897\ \text{kg m}^{-3}, 1750\ \text{K})$, its viscosity is about 2.08×10^{-4} Pa s, consistent with Fig. 5. Using the present study, the viscosity value of any alkali metal can be estimated in the range between T_m and 20 T_m, and between ρ_m and $2\rho_m$.

In our previous study, we also investigate the validity of Stokes-Einstein relation

$$D = \frac{k_B T}{C\pi\eta R}, \tag{13}$$

where D is the self-diffusion coefficient. We concluded that this relation is valid in the case of sodium over the investigated states, provided $C = 3.6$ and R identifies with Wigner-Seitz radius, which is proportional to $\rho^{-1/3}$. The universality of the self-diffusion coefficient has already been questioned at ambient pressure [10,11,66] and our study extends this topic to high pressures. If we consider for instance the reduced thermodynamic state $(1.5\rho_m;\ 4\,T_m)$, corresponding to (778.5 kg m^{-3}; 1790 K) and (2752.5 kg m^{-3}; 1200 K) for Li and Cs, respectively, we can estimate from Eq. (10) the viscosity value for these two metals (3.05×10^{-4} and 2.99×10^{-4} Pa s, respectively). Using Eq. (13), we obtain estimates of the self-diffusion coefficient for this thermodynamic state ($D_{SE}^{\text{Li}} = 4.69 \times 10^{-8}$ m^2 s^{-1} and $D_{SE}^{\text{Cs}} = 1.83 \times 10^{-8}$ m^2 s^{-1}), in very good agreement with the values obtained directly from our simulations using the MSD after correcting for finite size effects (namely, $D_{MD}^{\text{Li}} = 4.76 \times 10^{-8}$ m^2 s^{-1} and $D_{MD}^{\text{Cs}} = 1.76 \times 10^{-8}$ m^2 s^{-1}).

V. CONCLUSION

We studied the universality of shear viscosity of alkali metals by equilibrium molecular dynamics simulations over a wide range of density, including the very high-density region. To investigate this part of the phase diagram, it was required to check the reliability of the interactions and Fiolhais potential has shown its validity up to 12, 9.4, 6.6, and 3 GPa for Na, K, Rb, and Cs, respectively, and to a lesser extent up to 4.8 GPa for Li. A comparison between experimental and simulated shear viscosity was done and the agreement is very good. Even if part of the discrepancies may arise from the interionic potential, an updating of the experimental data is needed. Indeed, the study of Genrikh [54], which is the most recent on viscosity, has shown that part of the difference is certainly due to gaseous impurities contained in the sample during measurements.

The same qualitative behavior of the viscosity was found for all alkali. Along isochoric lines, viscosity presents a clear minimum as temperature increases, except at the lowest densities investigated. Along isotherms, it monotonically increases with the density. A universal behavior was found along the liquid-gas coexistence curve, but also along the isochors corresponding to ρ_m and 1.5 ρ_m up to a temperature of 7 T_m. Concerning isochors in the low-density region of the phase diagram, it seems difficult to unify the viscosity behavior of the different alkali elements. The different temperature and density ratios between melting and critical points may be responsible for these differences.

Thanks to Eqs. (10), (11), or (12), a reduced viscosity is obtained which permits to deduce the viscosity of any alkali elements along any isotherm or isochor, or at any thermodynamic state in this region of the phase diagram. Along an isotherm, for densities greater than 0.85 ρ_m, the viscosity appears to be a universal property up to a density corresponding to 1.5 ρ_m, density at which the electronic structure of alkali metals begins to change. Among the five alkali metals, lithium does not follow so accurately the universal behavior. This surely has to be related to its unique electronic structure, but anyway, differences remain small.

Finally, as many other physical properties, viscosity has a universal behavior over a wide range of the phase diagram. This is particularly useful since, as we explained, the knowledge of a given property for one of the alkali element allows to estimate the same property in corresponding thermodynamic states for all the others. This possibility should also apply to self-diffusion coefficient.

ACKNOWLEDGMENTS

The PMMS (Pôle Messin de Modélisation et de Simulation) is greatly acknowledged for providing us with computer time. We are grateful to T. Bryk for sending us his *ab initio* data.

APPENDIX

In this section, as well as in the article, Hartree atomic units are used ($m_{e-} = e = \hbar = a_0 = 2$ Ryd $= 1$). Some cited references using Rydberg atomic units ($2m_{e-} = e^2/2 = \hbar = a_0 = 1$ Ryd $= 1$), corresponding original expressions have been converted. Let us denote $\rho_N = N/V$ and $n = ZN/V = Z\rho_N$, the atomic and electronic densities, respectively. The electronic sphere radius, r_s, can be obtained from $4\pi r_s^3/3 = 1/n$.

Due to the electron gas, expressions of thermodynamic quantities such as energy or pressure in metals are different than in Lennard-Jones fluids for instance. At the second-order of perturbation in the framework of screened pseudopotential formalism, the total energy reads

$$\begin{aligned} E &= E_k + U(V) + U(R,V) \\ &= \frac{3}{2}Nk_BT + Nu_0(n) + 2\pi N\rho_N \int_0^\infty r^2 u(r,n) g(r) dr. \end{aligned} \tag{A1}$$

The first term is the kinetic energy of ions. The potential energy splits into two contributions. The first one is a nonstructural density-dependent term stemming from the electron gas, while the second one is structure- and density-dependent. According to Jakse and Bretonnet [67] and Hasegawa [68],

$$u_0(n) = E_{\rm eg} - \frac{B_{\rm eg}}{2\rho_N} + \phi(r=0), \tag{A2}$$

where

$$E_{\rm eg} = \frac{Z}{2}\left[\frac{2.21}{r_s^2} - \frac{0.916}{r_s} + 0.031\ln(r_s) - 0.115\right] \tag{A3}$$

is the energy of the electron gas that can be estimated using Nozières and Pines [69] formula. The electron gas bulk modulus $B_{\rm eg}$ reads [70,71]

$$B_{\rm eg} = 4\pi n^2\left[\frac{\pi}{4k_F} - \frac{\gamma_0(r_s)}{k_F^2}\right], \tag{A4}$$

where k_F is the Fermi wave vector and γ_0 is defined as

$$\lim_{q\to 0} G(q) = \gamma_0 \frac{q^2}{k_F^2}. \tag{A5}$$

Finally,

$$\phi(r=0) = -\frac{Z^2}{\pi}\int_0^\infty F_N(q) dq, \tag{A6}$$

where $F_N(q)$ is defined in Eq. (7). All these expressions are consistent with the relations given in Ref. [62].

Turning to the pressure [72], it reads, for local pseudopotentials [68]:

$$P = P_{id} + P_0 + P_{i-i} = \rho_N k_B T + \rho_N n \frac{du_0}{dn} + P_{i-i}. \tag{A7}$$

The structural term is $P_{i-i} = P'_{i-i} + P''_{i-i}$ with

$$P'_{i-i} = -\frac{2\pi\rho_N^2}{3}\int_0^\infty r^3 \frac{\partial u(r,n)}{\partial r} g(r) dr \tag{A8}$$

and

$$P''_{i-i} = 2\pi\rho_N^2 \int_0^\infty n r^2 \frac{\partial u(r,n)}{\partial n} g(r) dr. \tag{A9}$$

The volume-dependent term $\rho_N n \frac{du_0}{dn}$ can be computed by numerically differentiating u_0. As for $(\rho_N k_B T + P'_{i-i})$, it also corresponds to the diagonal terms of the stress tensor.

Finally, it should be pointed out that due to the linear screening approximation and to the perturbation method, terms are lacking in the expression of the pressure. Therefore the evaluation of pressure is only approximate within the framework of these kinds of effective potentials.

[1] V. F. Degtyareva, Solid State Sci. **36**, 62 (2014).
[2] E. Mc Bride, Ph.D. Thesis, University of Edinburgh, 2013.
[3] Y. Ma, M. Eremets, A. R. Oganov, Y. Xie, I. Trojan, S. Medvedev, A. O. Lyakhov, M. Valle, and V. Prakapenka, Nature (London) **458**, 182 (2009).
[4] T. Abram and S. Lon, Energy Policy **36**, 4323 (2008).
[5] M. M. Adams, D. R. Stone, D. S. Zimmerman, and D. P. Lathrop, Progr. Earth Planet. Sci. **2**, 29 (2015).
[6] Y. Kono, C. Kenney-Benson, Y. Shibazaki, C. Park, G. Shen, and Y. Wang, Phys. Earth Planet. Inter. **241**, 57 (2015).
[7] N. Matsuda, H. Mori, K. Hoshino, and M. Watabe, J. Phys.: Condens. Matter **3**, 827 (1991).
[8] U. Balucani, A. Torcini, and R. Vallauri, Phys. Rev. A **46**, 2159 (1992).
[9] U. Balucani, A. Torcini, and R. Vallauri, Phys. Rev. B **47**, 3011 (1993).

[10] J.-F. Wax, R. Albaki, and J.-L. Bretonnet, Phys. Rev. B **65**, 014301 (2001).
[11] J.-F. Wax, R. Albaki, and J.-L. Bretonnet, J. Non-Cryst. Solids **312-314**, 187 (2002).
[12] G. Kaptay, Z. Metallkd. **96**, 24 (2005).
[13] N. Meyer, H. Xu, and J.-F. Wax, Phys. Rev. B **93**, 214203 (2016).
[14] N. Meyer, H. Xu, and J.-F. Wax, EPJ Web Conf. **151**, 04001 (2017).
[15] C. Fiolhais, J. P. Perdew, S. Q. Armster, J. M. MacLaren, and M. Brajczewska, Phys. Rev. B **51**, 14001 (1995); **53**, 13193(E) (1996).
[16] R. G. Chapman and N. H. March, Phys. Chem. Liq. **16**, 77 (1986).
[17] R. W. Ohse, *Handbook of Thermodynamic and Transport Properties of Alkali Metals* (Blackwell, Oxford, 1985).
[18] R. Winter, W. C. Pilgrim, and F. Hensel, J. Phys.: Condens. Matter **6**, A245 (1994).
[19] I. I. Naumov, R. J. Hemley, R. Hoffmann, and N. W. Ashcroft, J. Chem. Phys. **143**, 064702 (2015).
[20] C. L. Guillaume, E. Gregoryanz, O. Degtyareva, M. I. McMahon, M. Hanfland, S. Evans, M. Guthrie, S. V. Sinogeikin, and H.-K. Mao, Nat. Phys. **7(3)**, 211 (2011).
[21] Anne Marie J. Schaeffer, W. B. Talmadge, S. R. Temple, and S. Deemyad, Phys. Rev. Lett. **109**, 185702 (2012).
[22] Y. Feng, J. Chen, D. Alf, X. Li, and E. Wang, J. Chem. Phys. **142**, 064506 (2015).
[23] E. Gregoryanz, O. Degtyareva, M. Somayazulu, R. J. Hemley, and H.-K. Mao, Phys. Rev. Lett. **94**, 185502 (2005).
[24] M. Marques, M. I. McMahon, E. Gregoryanz, M. Hanfland, C. L. Guillaume, C. J. Pickard, G. J. Ackland, and R. J. Nelmes, Phys. Rev. Lett. **106**, 095502 (2011).
[25] J. B. Neaton and N. W. Ashcroft, Phys. Rev. Lett. **86**, 2830 (2001).
[26] M. Hanfland, I. Loa, and K. Syassen, Phys. Rev. B **65**, 184109 (2002).
[27] O. Narygina, E. E. McBride, G. W. Stinton, and M. I. McMahon, Phys. Rev. B **84**, 054111 (2011).
[28] R. Boehler and C.-S. Zha, Physica B+C **139**, 233 (1986).
[29] S. Falconi, L. F. Lundegaard, C. Hejny, and M. I. McMahon, Phys. Rev. Lett. **94**, 125507 (2005).
[30] M. P. Allen and D. J. Tildesley, *Computer Simulation of Liquids* (Oxford University Press, New York, 1989).
[31] J.-F. Wax and N. Jakse, Phys. Rev. B **75**, 024204 (2007).
[32] J.-F. Wax, Physica B (Amsterdam) **403**, 4241 (2008).
[33] J.-F. Wax and T. Bryk, J. Phys.: Condens. Matter **25**, 325104 (2013).
[34] M. Ross, L. H. Yang, and W.-C. Pilgrim, Phys. Rev. B **74**, 212302 (2006).
[35] Y. Ma, A. R. Oganov, and Y. Xie, Phys. Rev. B **78**, 014102 (2008).
[36] A. B. Belonoshko, N. V. Skorodumova, A. Rosengren, and B. Johansson, Phys. Rev. B **73**, 012201 (2006).
[37] T. Bryk, S. De Panfilis, F. A. Gorelli, E. Gregoryanz, M. Krisch, G. Ruocco, M. Santoro, T. Scopigno, and A. P. Seitsonen, Phys. Rev. Lett. **111**, 077801 (2013).
[38] T. Bryk, I. Klevets, G. Ruocco, T. Scopigno, and A. P. Seitsonen, Phys. Rev. B **90**, 014202 (2014).
[39] A. Yamane, F. Shimojo, and K. Hoshino, J. Phys. Conf. Ser. **98**, 012024 (2008).
[40] G. Kresse and J. Hafner, Phys. Rev. B **47**, 558 (1993).
[41] G. Kresse and D. Joubert, Phys. Rev. B **59**, 1758 (1999).
[42] J. P. Perdew, A. Ruzsinszky, G. I. Csonka, O. A. Vydrov, G. E. Scuseria, L. A. Constantin, X. Zhou, and K. Burke, Phys. Rev. Lett. **100**, 136406 (2008).
[43] J.-Y. Raty, E. Schwegler, and S. A. Bonev, Nature (London) **27**, 448 (2007).
[44] F. F. Voronov, O. V. Stal'gorova, and E. L. Gromnitskaya, J. Exp. Theor. Phys. **95**, 77 (2002).
[45] I. I. Novikov, A. N. Soloviev, E. M. Khabakhnasheva, A. V. Gruzdev, A. I. Pridantzev, and M. Y. Vasenina, J. Nucl. Energy II **4**, 387 (1957).
[46] N. A. Kalakutskaya, Teplofiz. Vys. Temp. **6**, 455 (1968).
[47] E. N. Andrade and E. R. Dobbs, Proc. R. Soc. London A **1104**, 12 (1952).
[48] Y. Ito, K. Minami, and A. Nagashima, Int. J. Thermophys. **10**, 173 (1989).
[49] C. T. Ewing, J. A. Grand, and R. R. Miller, J. Phys. Chem. **58**, 1086 (1954).
[50] G. W. Thomson and E. Garelis, in *Physical and Thermodynamic Properties of Sodium*, ACS Monograph Series No. 133 (Reinhold, 1956), p. 12.
[51] A. W. Lemmon, H. W. Deem, E. H. Hall, and J. F. Walling, ORNL report **3605**, (1964).
[52] Y. S. Chiong, Proc. R. Soc. London A **157**, 264 (1936).
[53] W. D. Weatherford, R. K. Johnston, and M. L. Valtierra, J. Chem. Eng. Data **9**, 520 (1964).
[54] V. N. Genrikh and A. B. Kaplun, *Investigations of Thermophysical Properties of Substances, Novosibirsk, Nauka* 5 (1970).
[55] H. C. Tsai and D. R. Olander, High Temp. Sci. **6**, 142 (1974).
[56] A. V. Grosse, J. Inorg. Nucl. Chem. **28**, 795 (1966).
[57] A. Kasama, I. Takamishi, and Z. I. Morita, Trans. JIM **16**, 527 (1975).
[58] K. Meier, A. Laesecke, and S. Kabelac, J. Chem. Phys. **121**, 3671 (2004).
[59] Y. Rosenfeld, J. Phys.: Condens. Matter **11**, 5415 (1999).
[60] P. T. Cummings and G. P. Morriss, J. Phys. F **17**, 593 (1987).
[61] J. B. Neaton and N. W. Ashcroft, Nature (London) **400**, 141 (1999).
[62] J.-F. Wax, R. Albaki, and J.-L. Bretonnet, Phys. Rev. B **62**, 14818 (2000).
[63] E. A. Guggenheim, J. Chem. Phys. **13**, 253 (1945).
[64] F. Hensel, J. Phys.: Condens. Matter **2**, SA33 (1990).
[65] F. Hensel and H. Uchtmann, Annu. Rev. Phys. Chem. **40**, 1 (1989).
[66] G. Kaptay, Int. J. Mater. Res. **99**, 14 (2008).
[67] N. Jakse and J.-L. Bretonnet, J. Phys.: Condens. Matter **7**, 3803 (1993).
[68] M. Hasegawa and M. Watabe, J. Phys. Soc. Jpn. **32**, 14 (1972).
[69] D. Pines and P. Nozières, *Quantum Liquids* (Benjamin, New York, 1966).
[70] A. A. Kugler, J. Stat. Phys. **12**, 35 (1975).
[71] S. Ichimaru, Rev. Mod. Phys. **54**, 1017 (1982).
[72] P. Ascarelli and R. J. Harrison, Phys. Rev. Lett. **22**, 385 (1968).